Compliant Formation Control of a Multi-Vehicle System

Dr. Erica Z. MacArthur, Dr. Carl D. Crane

***Abstract*— This research identifies a strategy called *compliant formation control*, which may be used to coordinate the navigational structure of a team of autonomous vehicles. This technique controls the team's motion based on a given, desired formation shape and a given, desired set of neighboring separation distances, wherein the formation shape is considered general two-dimensional. The strategy establishes how to select, place, and use virtual springs and dampers that conceptually "force" proper interspacing between neighboring team members. The objective is to continuously maintain, in the most optimal way, the desired formation as team motion proceeds. In practice, actual robot separation distances will be measured relative to smarter, leader robots that have known position and orientation information at all times (e.g., GPS or INS). The control strategy subsequently commands, in an optimal way, each vehicle by providing a heading and velocity necessary to maintain the desired formation. Such requisite commands result from modeling the compliant displacements of team members as they travel in a network of virtual springs and dampers. The equations used to achieve coordinated motion of the robot team will be discussed and specific case studies will be presented to demonstrate the effectiveness of the compliant formation control strategy.**

***Index Terms*— Autonomous, cooperative, formation control, ground robots, virtual spring.**

I. Introduction

Faster computing and new sensing technologies have rapidly advanced robotics research. As perception abilities improve, robotic agents can be used more often to perform monotonous and often dangerous tasks in place of human operators. Robots are currently being used to automate military and agricultural tasks. Robots working as teams can take existing technology one step further by allowing several robots to accomplish a series of tasks more efficiently than a single agent. Duplicating several inexpensive robots with different sensing abilities may prove to be more cost effective than a single robot performing the task.

The 1990s sparked an era in robotics that has created a lot of interest in robot teams. The concept of soccer-playing robots was first introduced in 1993. Since then competitions such as RoboCup soccer leagues and the DARPA Grand Challenge have become an international phenomenon in robotics education and research. The DARPA Grand Challenge competition proved to challenge the sensing and mobility of unmanned ground vehicles through rough desert terrain. The next generation of the Grand Challenge involves autonomous navigation through an urban environment and will challenge the vehicle's ability to make intelligent decisions.

Recently, the Air Force Research Laboratory (AFRL) has become interested in improving EOD range clearance operations and has employed tele-operated unmanned ground vehicles to assist in this task. However, due to the volatility of this task, operators can be several miles away from their targets which lead to problems with communication. Formation control of these unmanned systems is essential for autonomous convoys, search and rescue, and reconnaissance missions. This research investigates collaborative ground vehicles and formation control. The research vision is to apply basic principles to develop a methodology to determine behaviors for members of a robot team that will result in reliable formation coordination of the group.

E. Z. MacArthur, Innovative Automation Technologies, Gainesville, FL 32605 USA (phone: 352-219-3715; e-mail: emacarthur@iat-llc.com).

C. D. Crane, University of Florida, Gainesville, FL 32611 USA. (e-mail: ccrane@ufl.edu).

II. Background

A. Biological Inspiration

Swarms of insects have the innate ability to effectively collect food, travel, and raise young as a collective. Worker honeybees' very existence is to serve the needs of the colony as a whole. Swarm intelligence (SI) is modeled after this very phenomenon of cooperation of a biological system to achieve a collective goal. The concept of "swarm intelligence" was first introduced by Beni and Wang in 1989 [1]. SI systems are typically composed of a population of single agents that can interact with each other and their environment. Typically there is no centralized control strategy dictating how each individual agent should behave. Surprisingly, local interactions of individual agents lead to the emergence of global behavior which mimics natural systems such as bee colonies, fish schooling, and bird flocking.

In an effort to build a more perfect robotic system, researchers and designers strive to imitate nature. Ant-like task allocation and recruitment have been applied to cooperative robots [2]. This research addressed the benefit of cooperative robots working together to single robots working in solitary. The task of foraging was assigned to the robot colonies to investigate whether ant-derived algorithms affect the robot cooperation. The ant-like behaviors have been applied to optimization problems such as the traveling salesman problem, quadratic assignment, and scheduling [3].

The model developed provides positive feedback which allows for rapid discovery of solutions, and distributed computation avoids premature convergence. The idea is that if an ant is given a choice among different paths, those which were heavily chosen by preceding ants are chosen with higher probability.

B. Robot Behaviors and Learning

A method of reactive navigation for mobile robots is presented in Arkin [4]. Reactive navigation systems are presented as being characterized by a decomposition of robotic goals into primitive behaviors, which are activated via arbitration; perceptual strategies which provide only information necessary for each activity, and the avoidance of global world models which yields faster real-time response while minimizing inter-robot communication.

Conversely, communication among the robot team can be an important feature that can be used to aid in coordination. The value-based communication preservation (VBCP) is a navigation behavior that takes into account shared locations of its teammates, measured communication signal quality and map-based predictions of communications signal quality to calculate movement vectors [5].

C. Towards Motion Coordination

In order to have coordinated groups of autonomous robots, they must be organized in some type of hierarchy. In addition, it is beneficial to have a task in which to base the research and experiments. Robotic convoy navigation research is a prime example of a formation control application. The research in this area considers a lead vehicle that is either manually driven or autonomous that is followed by a series of automated vehicles single-file. Early research considers basic operations of a convoy of vehicles whose formation control strategy is based on distance measurement [6,7]. Guidance law strategies [8] have been applied to derive control laws for angular and linear vehicle velocities such that a constant following distance is maintained.

In the research of Schneiderman [9] a vision-based autonomous convoy navigation technique is described in which a robotic vehicle is pursuing another by visually tracking a target mounted on the back of the pursued or lead vehicle. Other research applies visual servoing techniques [10, 11] for robot positioning, tracking, and estimating velocities.

Formation control of a system of mobile robots can often lead to other problems such as inter-robot collisions within the formation. This problem can be handled by placing constraints on the system of robots. The concept of a virtual robot and virtual robot tracking control [12] attempts to maintain clearance between the robots while navigating in formation. The presence of obstacles creates another layer of complexity in formation control. A combination of formation control and obstacle avoidance is achieved using input-to-state stability and a general formation keeping algorithm [13]. The robots are modeled as differential drive vehicles and the overall control is based on system stability to environmental perturbations.

III. Modeling Vehicle Dynamics and Kinematics

An Ackermann steering configuration allows only the front wheels of a vehicle to turn. In order to reduce the complexity of the problem the following constraints and assumptions are made: no lateral motion of any wheel, the front wheels turn at the same angle, the wheels roll without slipping. Figure 1 diagrams the vehicle geometry and all associated coordinate systems.

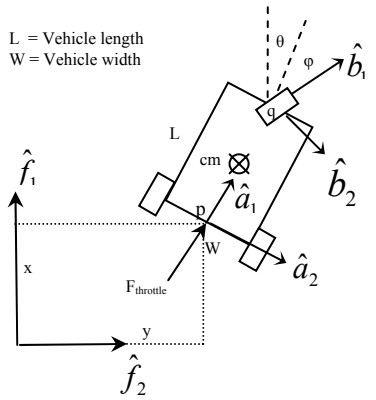

Fig. 1. Vehicle geometry and coordinate systems.

The vehicle is modeled after a tricycle in order to reduce the complexity of the analysis. This accounts for the assumption that both front wheels turn at the same angle. The generalized coordinates for the system are as follows:

q_1 = x: The position of point *p* in the $\hat{f}_1$ direction.

q_2 = y: The position of point *p* in the $\hat{f}_2$ direction.

The 'F' reference frame is the inertial frame, fixed to ground. The 'A' reference frame is fixed in the rear of the vehicle as shown in figure 1. Similarly, the 'B' reference frame is fixed in the front wheel. For this particular system, the throttle force is constrained to be in the $\hat{a}_1$ direction. A constraint is placed upon the velocity of point *p*. That is, the center point of the rear axle is constrained to move in the $\hat{a}_1$ direction. In addition, a constraint is placed upon the velocity of point *q* – the front wheel. Its velocity is constrained to be in the $\hat{b}_1$ direction. The following constraint equations are developed for point *p* and point *q*:

$$\overline{V}_p = V_p\hat{a}_1 = \sqrt{\dot{x}^2 + \dot{y}^2}\,\hat{a}_1 \tag{1}$$

$$\overline{V}_q = V_q\hat{b}_1 \tag{2}$$

These two equations constrain the velocity of the rear of the vehicle to be parallel to the rear wheels and the velocity of the front of the vehicle to be in the direction of the angle of the front wheel. Since points *p* and *q* lie in the same rigid body, the following velocity relationship applies to the rigid body:

$$\overline{V}_q = \overline{V}_p + {}^F\overline{\omega}^A \times \overline{r}_{p\to q} \tag{3}$$

$$\overline{V}_q = \overline{V}_p + \dot{\theta}\hat{a}_3 \times L\hat{a}_1 \tag{4}$$

$$\overline{V}_q = V_p\hat{a}_1 + L\dot{\theta}\hat{a}_2 = V_q\hat{b}_1, where: \hat{b}_1 = \sin\varphi\hat{a}_2 + \cos\varphi\hat{a}_1 \tag{5}$$

$$V_q\cos\varphi = V_p = \sqrt{\dot{x}^2 + \dot{y}^2} \tag{6}$$

$$V_q\sin\varphi = L\dot{\theta}, where: L\dot{\theta} = \tan\varphi\sqrt{\dot{x}^2 + \dot{y}^2} \tag{7}$$

This produces the following relationship:

$$\dot{\theta} = \frac{\tan\varphi\sqrt{\dot{x}^2 + \dot{y}^2}}{L} \tag{8}$$

It is assumed that the vehicle center of mass (cm) is located at the center of the vehicle as shown in figure 1. Since the center of mass and point *p* lie in the same rigid body, the velocity relationship is applied to the system:

$$\begin{aligned}\overline{V}_{cm} &= \overline{V}_p + {}^F\overline{\omega}^A \times \overline{r}_{p\to cm} \\ &= \sqrt{\dot{x}^2 + \dot{y}^2}\,\hat{a}_1 + \frac{\dot{\theta}L}{2}\hat{a}_2 = \sqrt{\dot{x}^2 + \dot{y}^2}\,\hat{a}_1 + \frac{\tan\varphi\sqrt{\dot{x}^2 + \dot{y}^2}}{2}\hat{a}_2\end{aligned} \tag{9}$$

The result is an expression for the magnitude of the velocity of the center of mass:

$$V_{cm} = \sqrt{\left(\dot{x}^2 + \dot{y}^2\right)\left(1 + \frac{\tan^2\varphi}{4}\right)} \tag{10}$$

The rigid body system is analyzed using Lagrange's method. Therefore, the kinetic and potential energy of the system are derived and the Lagrangian is developed:

$$L = T - V \tag{11}$$

$$L = \frac{1}{2}m\overline{V}_{cm}\bullet\overline{V}_{cm} + \frac{1}{2}{}^F\overline{\omega}^A\bullet[I]{}^F\overline{\omega}^A - 0 \tag{12}$$

$$T = \frac{1}{2}m\overline{V}_{cm}\bullet\overline{V}_{cm} + \frac{1}{2}{}^F\overline{\omega}^A\bullet[I]{}^F\overline{\omega}^A = \frac{1}{2}m\left(\dot{x}^2 + \dot{y}^2 + \frac{\tan^2\varphi\left(\dot{x}^2 + \dot{y}^2\right)}{4}\right) + \frac{1}{2}\dot{\theta}^2 I_{zz} \tag{13}$$

$$T = \frac{1}{2}\left(\dot{x}^2 + \dot{y}^2\right)\left[m + \frac{m\tan^2\varphi}{4} + I_{zz}\frac{\tan^2\varphi}{L^2}\right] \tag{14}$$

$$V = 0 \tag{15}$$

The kinetic energy of the system is composed of linear and rotational kinetic energy. This particular system undergoes no change in the z-direction which causes the potential energy term to become zero. The following Lagrange's equations are solved in order to obtain the equations of motion of the system:

$$\frac{d}{dt}\left(\frac{\partial L}{\partial \dot{q}_1}\right) - \frac{\partial L}{\partial q_1} = Q_1 \tag{16}$$

$$\frac{d}{dt}\left(\frac{\partial L}{\partial \dot{q}_2}\right) - \frac{\partial L}{\partial q_2} = Q_2 \tag{17}$$

where q_1 and q_2, the generalized coordinates, correspond to the *x* and *y* coordinates of point *p*.

The generalized forces, Q_1 and Q_2 are derived in the following manner:

$$Q_i = \sum_{i=1}^{2} \overline{F}\bullet\frac{\partial\overline{r}}{\partial q_i} \tag{18}$$

$$where: \overline{r} = x\hat{f}_1 + y\hat{f}_2$$

$$\frac{\partial\overline{r}}{\partial q_1} = \hat{f}_1, \frac{\partial\overline{r}}{\partial q_2} = \hat{f}_2$$

$$Q_1 = f_{throttle}\hat{a}_1\bullet\hat{f}_1 = f_{throttle}\left(\cos\theta\hat{f}_1 + \sin\theta\hat{f}_2\right)\bullet\hat{f}_1 \tag{19}$$

$$Q_1 = f_{throttle}\cos\theta, \quad Q_2 = f_{throttle}\sin\theta \tag{20}$$

The necessary differentiations are performed and then substituted into equations 16 and 17 in order to determine the equations of motion of the rigid body system. An equation of motion is derived for each generalized coordinate. The resulting equations of motion are:

$$\ddot{x}\left(m + \frac{m\tan^2\varphi}{4} + \frac{I_{zz}\tan^2\varphi}{L^2}\right) + \dot{x}\dot{\varphi}\left(\frac{m\tan\varphi}{2\cos^2\varphi} + \frac{2I_{zz}\tan\varphi}{L^2\cos^2\varphi}\right) = f_{throttle}\cos\theta \tag{21}$$

$$\ddot{y}\left(m + \frac{m\tan^2\varphi}{4} + \frac{I_{zz}\tan^2\varphi}{L^2}\right) + \dot{y}\dot{\varphi}\left(\frac{m\tan\varphi}{2\cos^2\varphi} + \frac{2I_{zz}\tan\varphi}{L^2\cos^2\varphi}\right) = f_{throttle}\sin\theta \tag{22}$$

The inputs to the system are the steering angle, φ, and the $f_{throttle}$ command. The system inputs and the initial conditions along with the equations of motion are used to simulate the motion of the vehicle over time. Integration of the acceleration equation will provide the velocity and position equations of the vehicle. These equations are used in the simulation to provide realistic motion of the simulated robots. It is interesting to note that there exists a singularity in the system when $\varphi = \pm 90°$. This implies that with the front wheel turned to either extreme (right or left), the vehicle cannot move and thus the equations of motion are indeterminate.

IV. Force Modeling and Formation Control Laws

A. Force Modeling

The formation of robots is modeled as a series of masses, virtual springs, and virtual dampers that stretch and compress based on the dynamics of the robot system. As the system of robots traverse throughout the environment the forces applied on each vehicle changes. It is hypothesized that addition of the dampers to the robot systems will reduce any oscillatory motion of the system.

The robot system consists of one leader vehicle and two or more follower vehicles. The interconnections of the system depend on the desired formation shape. A sample wedge and vee formation for a three-robot system with damping is shown in figure 2. There are forces acting on each vehicle due to the linear and torsional springs and forces due to the dampers.

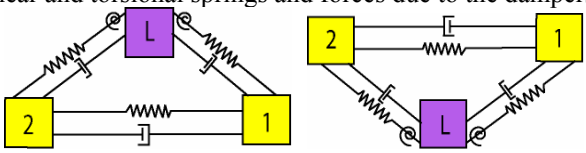

Fig. 2. Sample wedge and vee formation with damping.

The formation control algorithm is dependent on the forces that are applied to each individual robot as the system moves. The torsional spring connected to the leader provides the formation with orientation. The combination of the linear and torsional spring forces acting on each vehicle result in formation control laws for the entire robot system. The damper is introduced in order to reduce oscillatory motion of the robot system. The individual forces acting on each vehicle consist of forces due to the linear and torsional springs as well as the damper. A generic notation for the force equations were developed for the damper and each spring type. The generic linear spring force vector notation is presented as:

$$\overline{F_{ij}} = k_{ij}\left[\left(\left|\overline{L_{ij}}\right| - DL_{ij}\right)\left(\frac{\overline{L_{ij}}}{\left|\overline{L_{ij}}\right|}\right)\right] \tag{23}$$

Where $\overline{L_{ij}} = \overline{r_j} - \overline{r_i}$ and DL_{ij} is the desired length between vehicle i and vehicle j and where k_{ij} represents the linear spring constant between vehicle i and vehicle j.

The generic torsional spring force vector notation:

$$\overline{F_{t\_ij}} = \frac{k_{t\_ij}\left(\Delta\theta_{ij}\right)}{\left|\overline{L_{ij}}\right|}\left(\frac{\hat{k}\times\overline{L_{ij}}}{\left|\overline{L_{ij}}\right|}\right) \tag{24}$$

where

$$\Delta\theta_{ij}\hat{k} = \tan^{-1}\left(\frac{\left(\hat{u}_d\times\hat{L}_{ij}\right)\hat{k}}{\hat{u}_d\cdot\hat{L}_{ij}}\right) \text{ and } \hat{L}_{ij} = \frac{\overline{L_{ij}}}{\left|\overline{L_{ij}}\right|} \tag{25}$$

and where k_{t_ij} represents the torsional spring constant between vehicle i and j.

The generic force due to damping may be written as:

$$\overline{F_{D\_ij}} = c_{D\_ij}\left[\frac{\left(\left|\overline{L_{ij\_previous}}\right|-\left|\overline{L_{ij\_current}}\right|\right)}{\Delta t}\left(\frac{\overline{L_{ij}}}{\left|\overline{L_{ij}}\right|}\right)\right] \tag{26}$$

where c_{D_ij} represents the damping constant between vehicle i and j.

The diagram in figure 3 illustrates the desired vector between two vehicles. The resultant forces are calculated for each follower vehicle using equations 23–27. This system will have a desired spacing, or "follow distance" between the robots. Also, a desired "follow angle" will dictate the overall shape of the robot formation and is referenced from the lead robot's current heading.

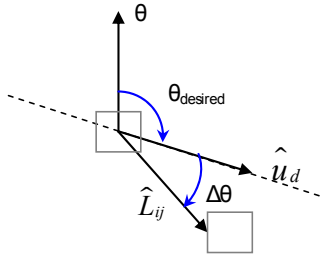

Fig. 3. Desired and actual vectors and angles for the follower robot.

$$\hat{u}_d = \cos\left(\theta \mp \theta_{desired}\right)\hat{i} + \sin\left(\theta \mp \theta_{desired}\right)\hat{j} \tag{27}$$

The resultant forces on robot 1 and robot 2 will consist of linear and torsional spring forces as well as a term due to damping. The corresponding resultant forces for robot 1 and robot 2 are in equations 28 and 29.

$$\overline{F_{1\_result}} = \overline{F_{1L}} + \overline{F_{12}} + \overline{F_{t\_1L}} + \overline{F_{D\_12}} + \overline{F_{D\_1L}} \tag{28}$$

$$\overline{F_{2\_result}} = \overline{F_{2L}} + \overline{F_{12}} + \overline{F_{t\_2L}} + \overline{F_{D\_12}} + \overline{F_{D\_2L}} \tag{29}$$

B. Formation Control Laws

The resultant force applied to the body is ultimately used to regulate the velocity and steering angle of the follower robots.

There are two layers of control that are applied to the robot system. The outer loop feedback layer controls the vehicle formation by regulating the applied force by commanding a desired velocity. The inner loop feedback layer tracks the desired velocity using throttle actuation. The controllers are conceptualized as in figure 4.

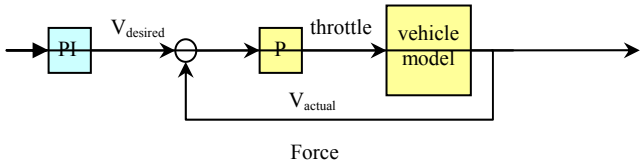

Fig. 4. Force and velocity control block diagram

The desired velocity controller utilizes a proportional-integral (PI) form of control. This form of control provides quick system response and drives the steady-state error to zero or nearly zero. The desired velocity command is based on the linearization and integration of the force error:

$$V_{desired} = k_p F_{res} + k_i \int F_{res} dt \tag{30}$$

The proportional term in equation 30 handles the transient response of the robot while the integral term is used to minimize the steady state error. Also, the integral term ensures that the desired velocity does not become zero.

Once the resultant force is calculated, a desired heading angle is calculated that is based on the components of this force. The steering command is derived from the angle between the resultant force vector and the vehicle heading vector. A proportional controller is used to control the steering angle of each of the follower vehicles.

As the system of robots traverse the desired trajectory, it is visually apparent if the robots can or cannot maintain formation. However, it is necessary to quantify and validate the ability of the robot system to maintain a formation. Since the system is modeled as a series of springs, masses and dampers it is advantageous to measure the potential energy of the system. As the system reaches equilibrium the potential energy will tend to zero and this indicates that the robots are in formation.

It is expected that for a system of robots in formation, the potential energy will have an initial overshoot and then proceed to track to zero or nearly zero. Slight errors may be introduced due to the dynamics of the system and will slightly affect the potential energy measurements.

V. Results

A. Straight Line Trajectory

The straight line trajectory was chosen because it is the simplest case that can be encountered in terms of path planning and navigation. It also provides the opportunity to troubleshoot the compliant formation control algorithm. That is, if the algorithm is not functioning for the simple case then it most likely will not perform well for a complicated situation. The balance between the stiffness of the structure and the responsiveness of the robots had to be determined in order to maintain the formation. The spring and damper constants were tuned in the same manner as controller gains. Results for this trajectory will be presented for the three and five robots in the vee and wedge formations with damping. A plot of the (x,y) positions of each vehicle as it traverses the trajectory is presented in the following figures.

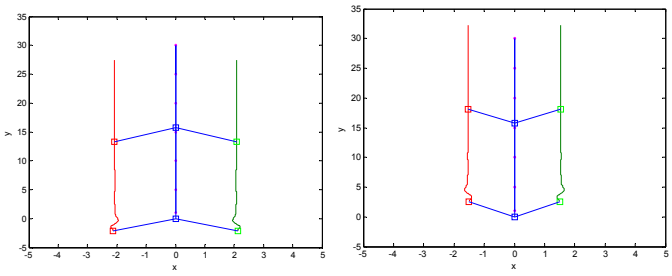

Fig. 5. Robot position plots for the wedge (left) and vee (right) formations. The lead robot is in the middle.

From figure 5 initial oscillations occur however, they are quickly eliminated due to the effect of the dampers that are incorporated into the system. The responsiveness of the follower robots is reduced due to addition of the dampers. This actually provides a benefit in that the follower robots are less likely to overshoot their desired positions within the formation.

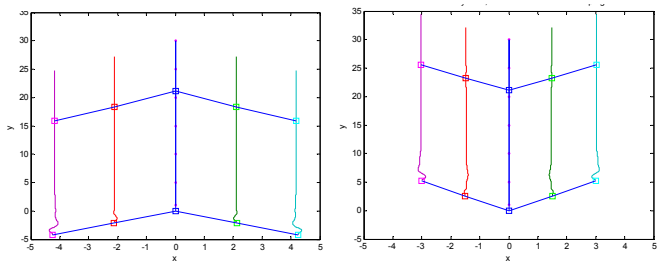

Fig. 6. Robot position plots for the wedge (left) and vee (right) formations. The lead robot is in the middle.

Similar to the three-robot system with damping, there are initial oscillations which are quickly eliminated. As the size of the robot system increases small oscillations propagate from one robot to the next and can result in an unstable or oscillatory system. Addition of damping to the system will minimize the oscillations of the system.

B. Racetrack Trajectory

After experimenting with the straight line trajectory and obtaining reasonable results, a more complicated trajectory was constructed. The racetrack trajectory consisted of straight segments and arcs and was designed to push the limit of the algorithm. The trajectory is shown in figure 7.

The complicated nature of this trajectory contributes to oscillations in the robot formation. However, the robot system is able to maintain the desired formation regardless. Again, the damping slightly reduces the oscillations of the follower robots. The three robot, wedge formation is shown in figure 8.

Due to the complex nature of this trajectory, it begins to become apparent that the vee formation is inherently unstable (see figure 9). The follower robots are ahead of the lead robot and this scenario can be likened to an inverted pendulum problem. As more follower robots are added the instability increases.

The final set of experiments involves the five-robot system on the racetrack trajectory. The results obtained from the vee formation did not dramatically reduce the system oscillations. This can be attributed to the inherently unstable nature of this type of formation. The results for the wedge formation and vee formation are shown in figures 10 and 11.

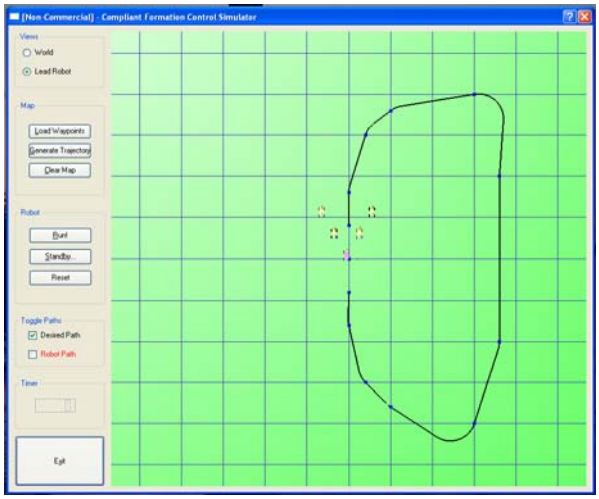

Fig. 7. Top-down view of the racetrack trajectory and simulator software.

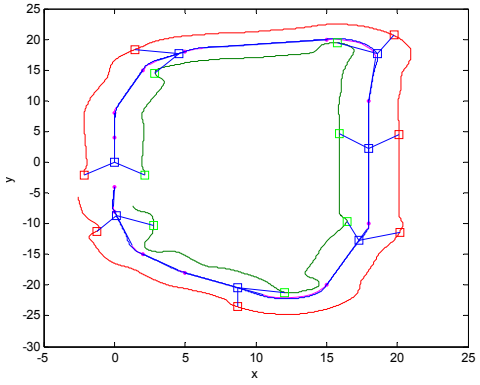

Fig. 8. Three robot wedge formation results.

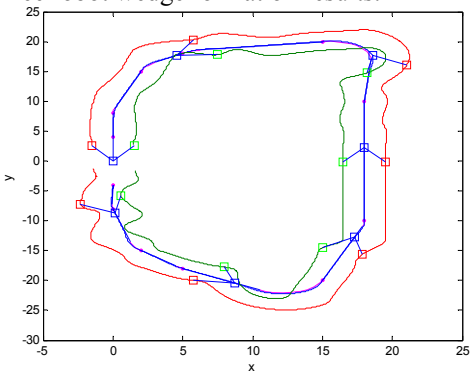

Fig. 9. Three robot vee formation results.

In order to further validate the compliant formation control algorithm, it is necessary to observe the potential energy. The robot system is modeled in terms of (virtual) springs, dampers, and masses (the robots). Therefore the same basic energy principles can be applied to the robot system. An indication that the system is at equilibrium occurs when the potential energy reaches zero. Therefore, as the robots file into formation the system reaches equilibrium and the potential energy will tend toward zero. An initial spike in the potential energy occurs due to the change in the robots' state.

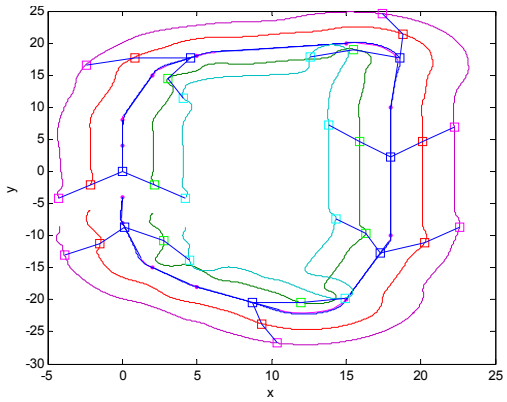

Fig. 10. Results obtained for the five robot system in the wedge formation.

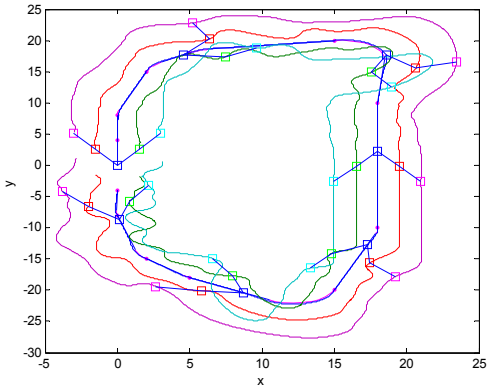

Fig. 11. Results obtained for the five robot system in the vee formation.

The potential energies are almost identical for both the vee and wedge formations for the three-robot system. In general, the five-robot systems have the highest potential energy with the vee formation having the highest for the straight line trajectory. The combination of two extra robots and an inherently unstable formation causes the increase in the potential energy for this case. Overall, the potential energy is approaching zero as is shown in figures 12 and 13.

VI. Conclusion

The compliant formation control has provided a viable methodology for formation control of a system of unmanned ground vehicles. The coordination technique is fast and robust enough to maintain a formation of a group of unmanned ground vehicles while in motion. The formation control methodology combines the principles of vehicle dynamics and structural dynamics into a versatile, scalable algorithm. The potential energy results presented an additional method to quantify the robot system's ability to maintain the formation.

References

[1] Beni, G., Wang, J., Swarm Intelligence, NATO Advanced Workshop on Robots and Biological Systems, Il Ciocco, Tuscany, Italy, 1989.

[2] Krieger, M., Billeter, J.B., Keller, L., Ant-like Task Allocation and Recruitment in Cooperative Robots, Nature, 2000, 406:992-995.

[3] Dorigo, M., Maniezzo, V., The Ant System: Optimization by a Colony of Cooperating Agents, IEEE Transactions on Systems, Man, and Cybernetics-Part B, 1996, 26:1-13.

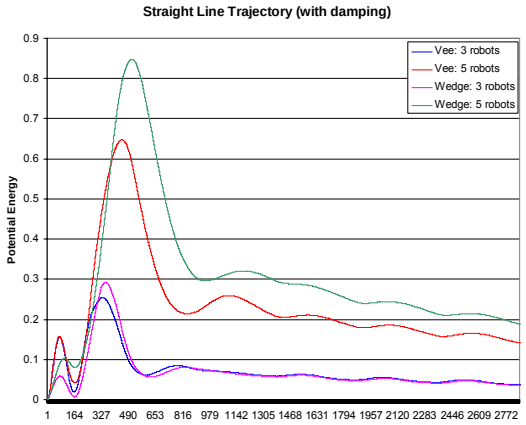

Fig. 12. Potential energy plots for the straight line trajectory.

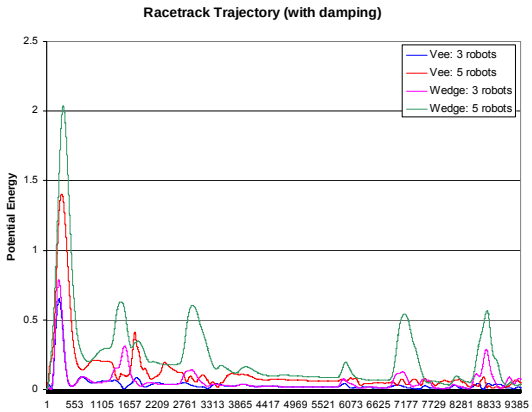

Fig. 13. Potential energy plots for the racetrack trajectory.

[4] Arkin, R., Cooperation Without Communication: Multiagent Schema-Based Robot Navigation, Journal of Robotic Systems, 1995, 9(3):351-364.

[5] Powers, M., Balch, T., Value-Based Communication Preservation for Mobile Robots, Presented at the 7th Annual International Symposium on Distributed Autonomous Robotic Systems, Toulouse, France, 2004.

[6] Mäkelä, H., Kaarmila, P., Koskinen, K., Convoy Navigation, In Proceedings of 3rd Symposium on Intelligent Autnomous Vehicles, Madrid, Spain, 1998, 1:31-36.

[7] Canudas-de-Wit, C., NDoudi-Likoho, A., Nonlinear Control for a Convoy-Like Vehicle, Automatica, 2000, 36:457-462.

[8] Belkhouche, F., Belkhouche, B., Modeling and Controlling a Robotic Convoy Using Guidance Laws Strategies, IEEE Transactions on Systems, Man, and Cybernetics-Part B: Cybernetics, 2005, 35(4):813-825.

[9] Schneiderman, H., Nashman, M., Wavering, A., Lumia, R., Vision-Based Robotic Convoy Driving, Machine Vision and Applications, 1995, 8:359-364.

[10] Stella, E., Lovergine F., D'Orazio, T., Distante, A., A Visual Tracking Technique Suitable for Control of Convoys, Pattern Recognition Letters, 1995, 16:925-932.

[11] Chaumette, F., Rives, P., Espiau, B., Positioning of a Robot with Respect to an Object, Tracking it and Estimating its Velocity by Visual Servoing, In Proceedings of IEEE International Conference on Robotics and Automation, Sacramento, CA, 1991, pp. 2248-2253.

[12] Jongusuk, J., Mita, T., Tracking Control of Multiple Mobile Robots: A Case Study of Inter-Robot Collision-Free Obstacle Avoidance, In Proceedings of IEEE International Conference on Robotics and Automation, Seoul, Korea, 2001, pp. 2885-2890.

[13] Ögren, P., Leonard, N. E., Obstacle Avoidance in Formation, In Proceedings of IEEE International Conference on Robotics and Automation, Taipei, Taiwan, 2003, pp. 2492-2497.J. Wang, "Fundamentals of erbium-doped fiber amplifiers arrays (Periodical style—Submitted for publication)," *IEEE J. Quantum Electron.*, submitted for publication.